16TH EUROPEAN CONFERENCE ON EARTHQUAKE ENGINEERING THESSALONIKI 18 - 21 JUNE 2018

FAILURE MODE INVESTIGATION FOR HIGH VOLTAGE PORCELAIN INSULATORS

Tansu GOKCE[1], Engin ORAKDOGEN[2], Ercan YUKSEL[3]

ABSTRACT

High-voltage porcelain insulators are vulnerable components of the electrical substations during strong seismic events. The direct and indirect losses due to interruption of the power supply creates unconceivable expenses. The possible collapse mechanism of the porcelain insulators were investigated in this study. The 550 kV high voltage post insulator parts were tested with two different moment-to-shear ratios in the Structural and Earthquake Engineering Laboratory (STEELab) of Istanbul Technical University. Two different collapse modes were obtained from the specimens. Finite element model of one of the specimens was generated by using solid members for porcelain, cement based grout and cast iron. The initial stiffness and stresses at the base level were compared between the numerical and experimental results.

Keywords: High voltage equipment; Porcelain insulator; Seismic safety

1. INTRODUCTION

Porcelain insulators are one of the most vulnerable part of the substations during strong earthquakes. Electrical substation components were heavily damaged during the earthquakes occurred in 1990's. It is difficult and expensive to repair and retrofit them without interruption in the service. The retrofitting cost including indirect charges due to interruption of the power supply is substantial. After the earthquakes, 1994 Northridge/USA, 1995 Kobe/Japan, 1999 Izmit/Turkey and 1999 Chi-Chi/Taiwan, the costs of losses with direct charges are in the range of hundreds of millions of dollar for each event (Filiatrault and Matt 2006). For instance, after the 1999 Izmit/Turkey earthquake, electricity service was restored within a day but the total cost of the damage was about US$70 million (Tang 2000).

The commonly observed failure modes are large shear and flexural cracks at the base section. For some instances, the failure starts at mid-height section and propagates up and down. Hereafter the insulator destroys completely.

Takhirov et al. (2017) experimentally tested 245kV post insulators and developed a finite element model to verify the test results. They specified the lateral stiffness predicted by finite element analysis is much greater than the experimental results. The finite element model can lead to a significant underestimation of peak top displacements of the insulators required by IEEE-693 (2006). Moustafa and Mosalam (2016) tested several ceramic and composite insulators and determined the failure load and the corresponding displacements and stresses. Mohammadpour and Hosseini (2017) tested a 63 kV post insulator and developed a finite element model for numerical analyses. They calibrated the finite element model by using the test results and produced the fragility curves.

The main objective of this study is to determine the collapse mechanism of the porcelain insulators. For this aim, quasi-static tests were performed on the porcelain insulator posts to determine the

[1]PhD Cand., Graduate School of Science Engineering and Technology, ITU, Istanbul, Turkey, gokcet@itu.edu.tr
[2]Prof. Dr., Civil Engineering Faculty, Istanbul Technical University, Istanbul, Turkey, orak@itu.edu.tr
[3]Prof. Dr., Civil Engineering Faculty, Istanbul Technical University, Istanbul, Turkey, yukselerc@itu.edu.tr

failure modes and the collapse loads. A 550 kV post insulator, which contains 3 posts, was tested in two phases due to height limitation of the testing facility. Specifically, Specimen #1 consists of two insulator posts with 2.825m total height, Specimen #2 is a single post with 1.81m height.

2. QUASI-STATIC TESTS OF THE PORCELAIN INSULATORS

Quasi-static cyclic tests were performed on two dissimilar porcelain insulator posts to determine their failure modes and collapse loads. The distinctive feature of the specimens is moment-to-shear ratio. The flexural behavior was dominant for Specimen #1. It was anticipated that the shear behavior was more effective on the response of Specimen #2.

The testing protocol which is based on the expected ultimate drifts was selected in accordance with the recommendations of FEMA-461, (FEMA-461, 2007). The displacement pattern was derived by multiplying "a_i/a_{10}" ratios with the ultimate top displacement. Ten distinct displacement targets are existing in the pattern and two full cycles are applied for each of them. The complete loading pattern is presented in Figure 1.

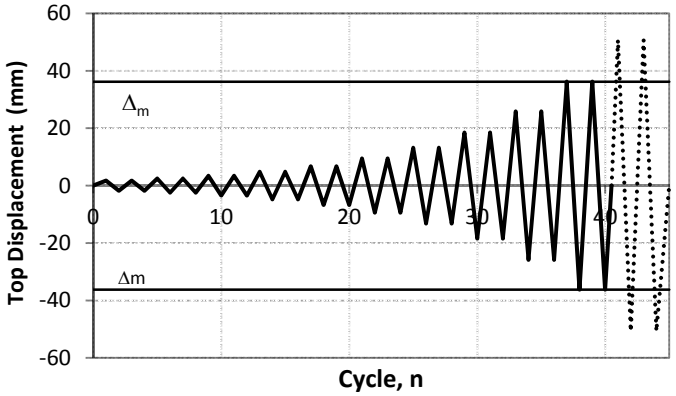

Figure 1. Cyclic displacement loading pattern

Ultimate top displacement was calculated as Δ_m=36.2 mm, that is corresponding to the collapse load given by the manufacturer.

2.1 *Quasi-static test of specimen #1*

Specimen #1 consists of two segments. The bottom and top posts have 1.1m and 1.4m heights, respectively. The total cantilever height was 2.825m. Solid core diameters of the posts are decreasing from bottom to top and the diameters are D_1=180, D_2=160 and D_3=140.

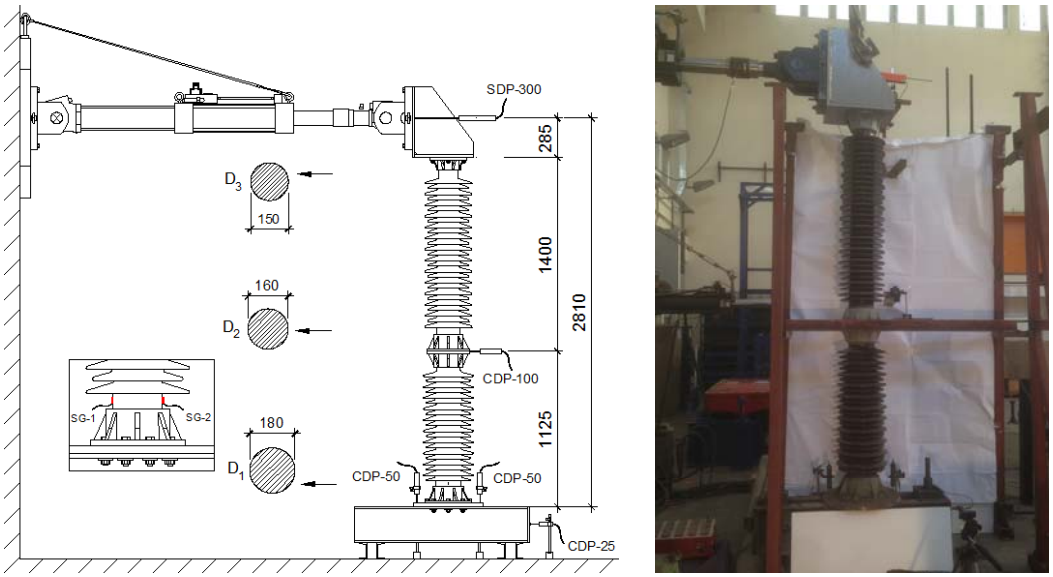

Figure 2. Specimen #1 testing set-up

The experimental testing set-up is presented in Figure 2. The specimen was rigidly attached to a steel frame. The loading pattern given in Figure 1 was applied to the specimen by a MTS hydraulic actuator. The insulator was instrumented by straingauges at the bottom section to measure tensile and compressive deformations. Various displacement components were measured by the displacement transducers.

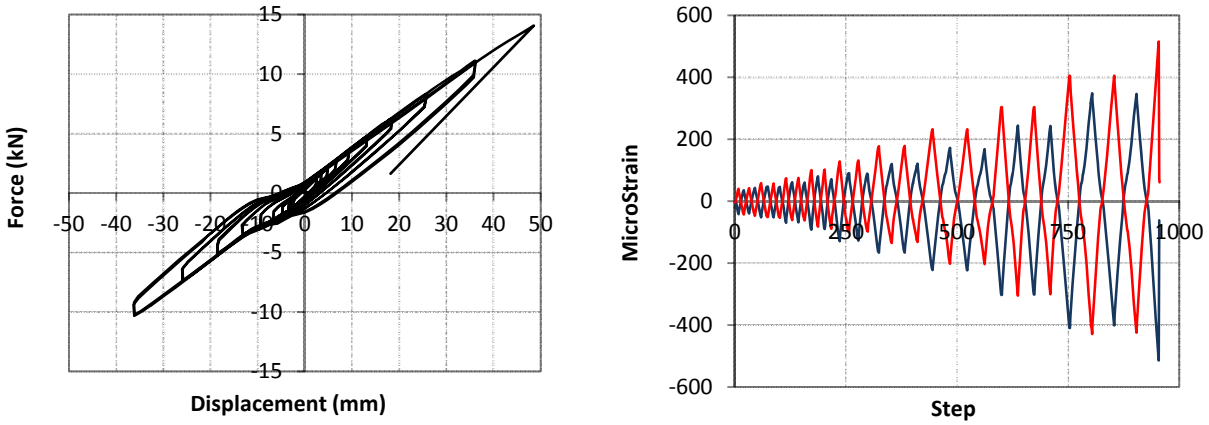

a. Force - displacement history

b. Strain-gauge measurements

Figure 3. Specimen #1 force displacement hysteresis and straingauge measurements on the bottom section

The full force-displacement relationship obtained from the test is shown Figure 3a. The relation comprises some extent of nonlinearity that is alike the observations made by Takhirov, et al. (2005). Straingauge measurements from the bottom section are presented in Figure 3b. It is seen that the strains measured in the tension and compression sides were considerably symmetrical. The failure load, and the corresponding displacement and stains were determined as 14.07 kN, 48.15 mm and 515 micro strains, respectively.

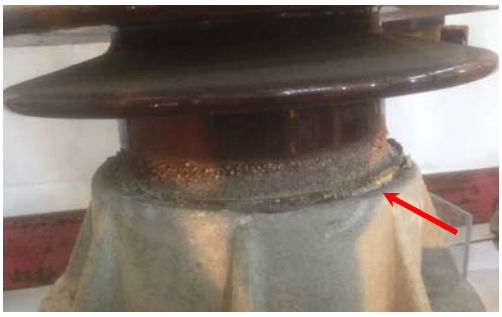

Figure 4. Grout failure between the porcelain and cap plate

The post-insulator failed from its mid-height section (D_2) that also experienced by the other researchers, Figure 5. In the early cycles of the test, some cracks were observed on the cement based grout placed between the cap plate and solid core. It was observed crushing of grout at the late stage of the test, Figure 4. Grout was completely destroyed just before the ending of the test. The damages about grout were more serious at the middle section (D_2).

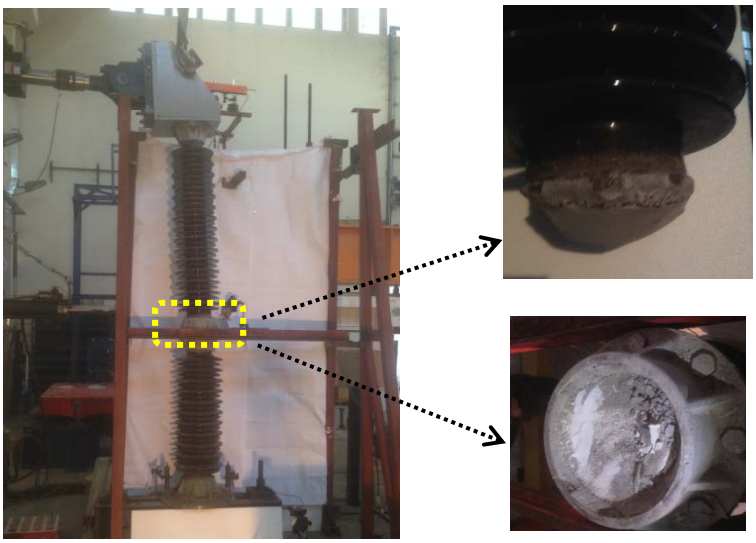

Figure 5. Specimen #1 failure mechanism

The failure modes Specimen #1 is presented in Figure 5. The bending stresses are calculated by using the corresponding moments and sectional constants for bottom section D_1 and the middle section D_2. The bending moments were calculated by multiplying the actuator force and the consistent distance. The stresses are given in Equation 1 and 2. The bending stresses at the bottom section (D_1) is bigger than the ones of the middle section (D_2). However, the failure was observed at the middle section (D_2). This may be attributed the observed damages of grout.

$$\sigma_1 = \frac{M_1}{W_1} = 65.38\ \mathrm{N/mm^2} \quad (1)$$

$$\sigma_2 = \frac{M_2}{W_2} = 54.58\ \mathrm{N/mm^2} \quad (2)$$

where W_1 and W_2 are section modulus of the porcelain core.

Modulus of elasticity of porcelain was extracted from Equation 3 in which stress (σ) was determined from Equation 1 and 2 and strain (ε) was determined from the straingauge measurements.

$$E_1 = \frac{\sigma}{\varepsilon} = 125668\ \mathrm{N}/mm^2 \quad (3)$$

The lateral displacement distribution through the height is illustrated in Figure 6 for 36.3 mm top displacement. Its components were δ_1 =24.41 mm and δ_2 =11.89 mm. The distribution was effected from the flexibility of the mid connection. The overall response of the specimen was affected from the grout behavior.

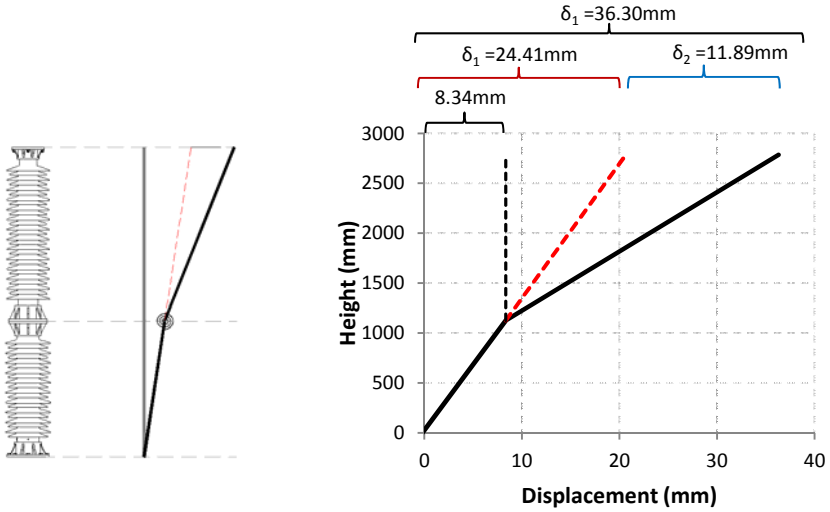

Figure 6. Displacement distribution of Specimen #1

2.2 *Quasi-static test of Specimen #2*

Specimen #2 was a single insulator post with 1.5m height. Because of the connection detail of the actuator, the moment arm was 1.81 m. Solid core diameter of the post decreases from bottom (D_1=150 mm) to top (D_2=140 mm).

The experimental testing set-up is presented in Figure 7. The displacement pattern given in Figure 1 was applied by MTS hydraulic actuator. Displacement transducers and straingauges were utilized to measure the significant quantities.

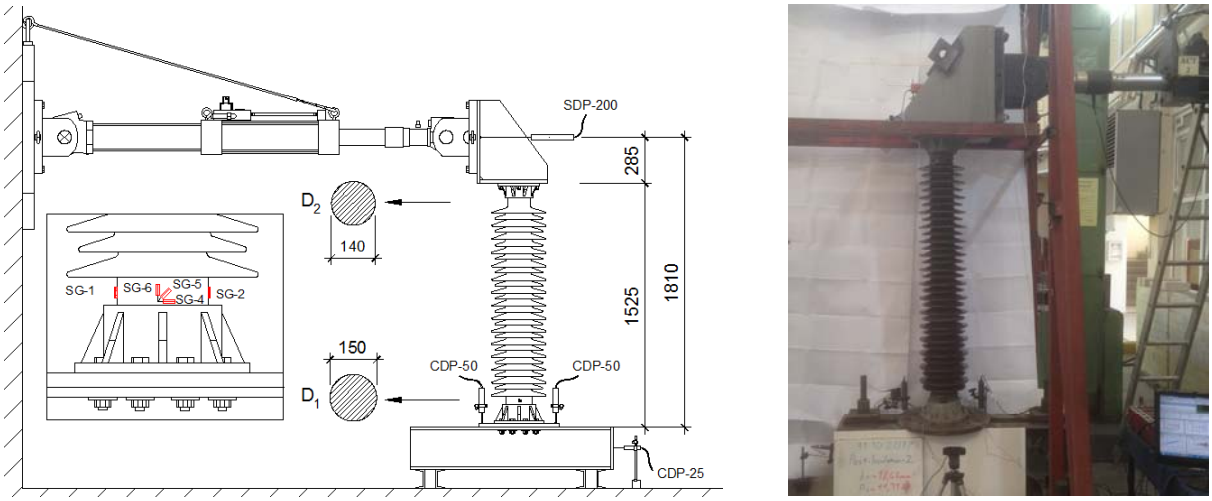

Figure 7. Specimen #2 testing set-up

Actuator force versus top displacement relation for Specimen #2 is presented in Figure 8a. Moreover, straingauge measurements at the bottom section are illustrated in Figure 8b. It is observed that the strain measurements at tension and compression side were considerably symmetrical. The reached failure load, and the corresponding displacement and strain values were 16.55 kN, 33.054 mm and 972 microstrain, respectively.

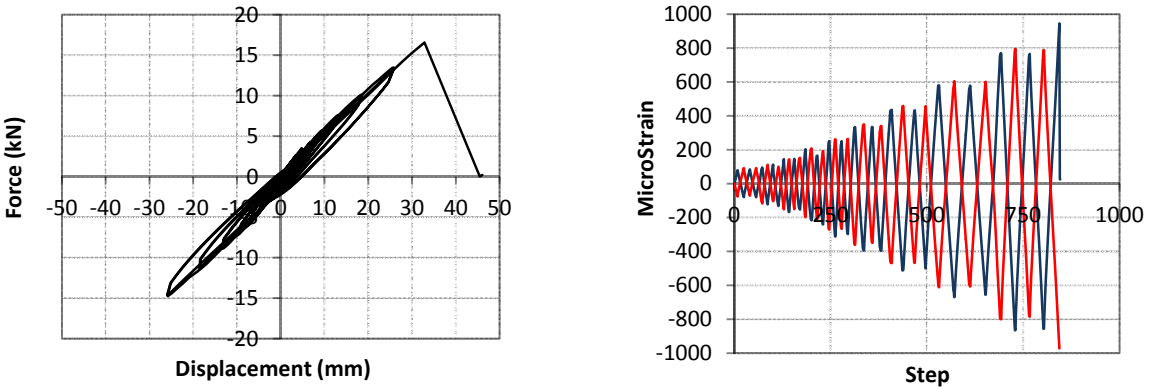

a. Force - displacement history

b. Strain-gauge measurements

Figure 8. Specimen #2 force displacement hysteresis and bending strain measurements on bottom section

The failure mode of Specimen #2 was very brittle. Four scenes of the video record are demonstrated in Figure 9. From the figures, it was understood that the failure started at the base section and spread to span quickly. The observed failure mode is comparable with the one stated by Takhirov et al. (2017).

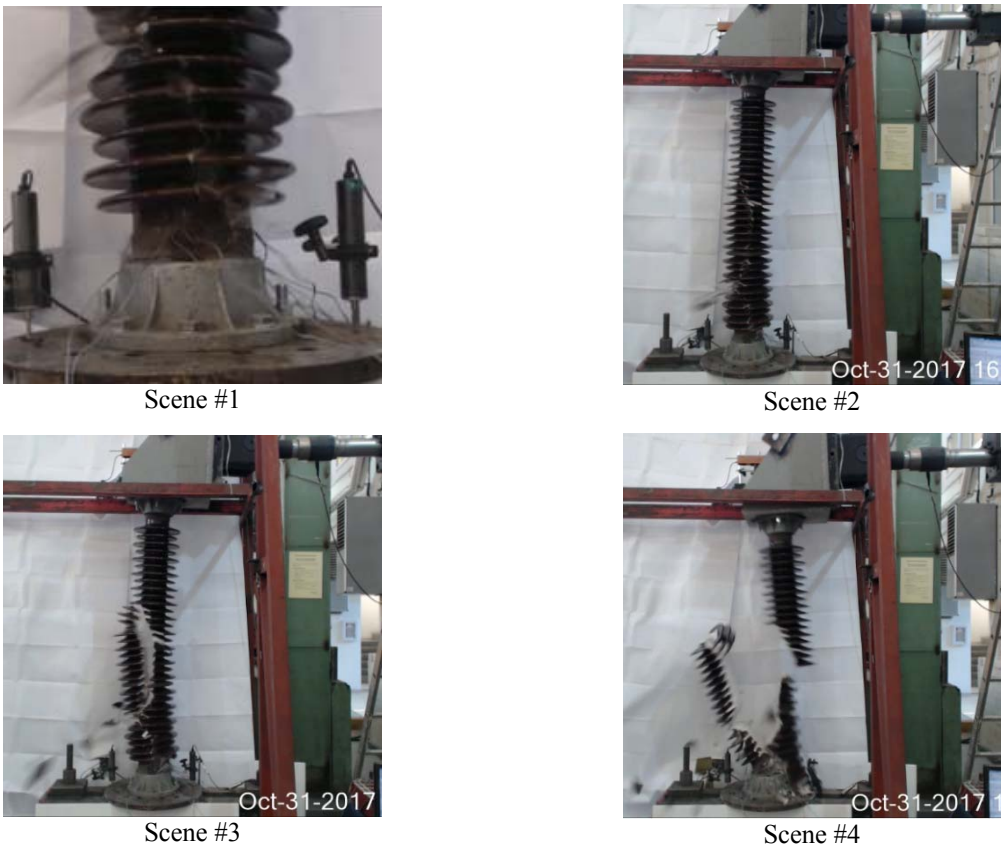

Scene #1

Scene #2

Scene #3

Scene #4

Figure 9. Four scenes from the failure of Specimen #2

The maximum axial stress at the extreme fiber of the base section is calculated in Equation 4.

$$\sigma_1 = \frac{M_1}{W_1} = 90.45\ N/mm^2 \quad (4)$$

Modulus of elasticity of porcelain was calculated from Equation 5. Where stress (σ) was determined from Equation 4 and strain (ε) was determined from the straingauge measurements.

$$E_2 = \frac{\sigma}{\varepsilon} = 123061\ N/mm^2 \quad (5)$$

The calculated E_1 and E_2 values are considerably close each other.

3. FINITE ELEMENT ANALAYSIS

Finite element model of Specimen #2 was developed in SAP2000 by using the solid member, see Figure 10. The model consists of three parts:
Part 1: Top and bottom flanges that were made of cast iron. Modulus of elasticity of the cast iron was assumed as 157000 N/mm^2 based on IEEE 693 (2006).
Part 2: Porcelain part. Modulus of elasticity of porcelain was taken as 125000 N/mm^2 depending on the experimental results.
Part 3: Grout layer between cast iron caps and porcelain.

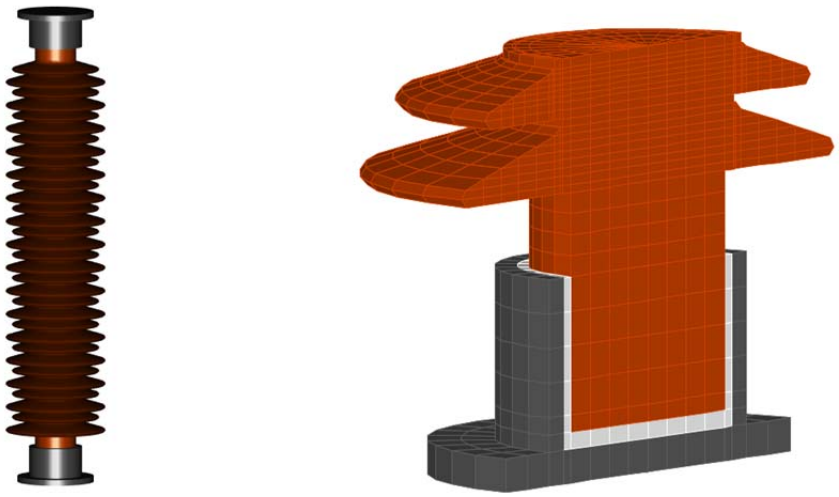

a. 3D finite element model b. A section from the finite element model

Figure 10. FE model of Specimen #2

Linear elastic stress analyses were performed by using the generated numerical model. The model was calibrated by using the experimental results. An iterative process was applied on *Part 3* while modulus of elasticities of *Part 1* and *Part 2* were kept constant. Henceforth, a value of 9000 N/mm^2 was determined for modulus of elasticity of *Part 3*.

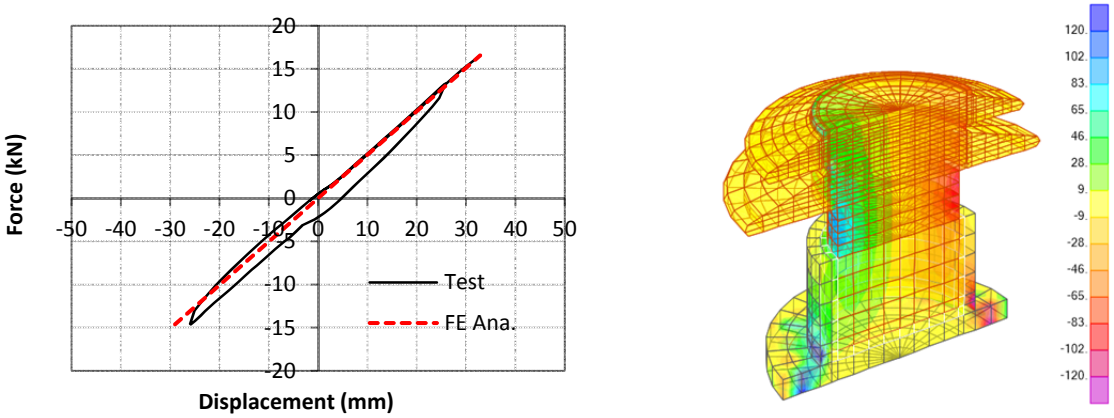

a. Force-displacement relations

b. Axial stress contours from FEA at the ultimate force (16.55 kN)

Figure 11. FE analysis results of Specimen #2

The results of the calibrated numerical model are illustrated in Figure 11 together with the experiment results. Slope of the force displacement curves are comparable, see Figure 11a. The maximum axial stresses obtained from the experiment (90.45 N/mm^2) and the numerical studies (94.18 N/mm^2) are quite consistent with each other.

4. CONCLUSIONS

550 kV high voltage post insulator parts were tested by using quasi-static test procedure to determine the possible failure mechanisms. Also, linear elastic stress analyses were accomplished after calibration of the model with the experimental results. The following conclusions were drawn:

- The distinct failure modes were obtained for the tested specimens.
- The failure mode of Specimen #2 in which moment-to-shear ratio is lower, was very brittle.
- Modulus of elasticity values (about E=125000 N/mm^2) determined for porcelain are quite similar for Specimens #1 and #2. However modulus of elasticity was obtained as E=70000 N/mm^2 in the free vibration tests (Gökce 2018). The value comprises the effects of the joints.
- Because of the accumulated damages in grout, large lateral displacements were measured in Specimen #1. Subsequently, the possible reason of the collapse of Specimen #1 is the crushing of grout at the middle section (D_2).
- Although IEEE-693 recommends that grout material must be rigid enough to transfer the compressive loads, it was not specified any minimum value.
- The collapse load that is generally supplied by manufacturer is not enough to generate a robust numerical model. In its place, the full force-displacement relation should be supplied.

As a last conclusion, joint flexibility of the post insulator should be considered in estimation of the general behavior.

5. ACKNOWLEDGMENTS

First author was sponsored by Bideb 2211 Program of Turkish Scientific and Technological Research Council (TUBITAK) and Research Project 39552 of Istanbul Technical University Research Funds. 550 kV HV post insulators were supplied by Gural Electric company. All of these supports are gratefully acknowledged. The study was carried out in the Structural and Earthquake Engineering Laboratory of ITU (STEELab). The authors thank to the laboratory staff.

6. REFERENCES

Gokce, T (2018). Seismic Safety of Electrical Equipment, *Ph.D. Thesis*, Faculty of Civil Engineering, Istanbul Technical University, Turkey.

FEMA 461 (2007), Interim Testing Protocols for Determining the Seismic Performance Characteristics of Structural and Non-structural Components, Applied Technology Council, California.

Filiatrault, A. and Matt, H. (2006) Seismic Response of High Voltage Electrical Transformer-Bushing Systems, *Journal of Structural Engineering,* 132-2: 287-295.

IEEE Standard 693 (2006), recommended practice for seismic design of substations, IEEE Standard Department, Piscataway, NJ.

Mohammadpour, S. and Hosseini, M. (2017), Experimental System Identification of a 63kV Substation Post Insulator and the Development of Its Fragility Curves by Dynamic Finite Element Analyses, *Earthquake Spectra*, 33-3: 1149–1.

Moustafa, M. A., and Mosalam, K. M. (2016), Structural Performance of Porcelain and Polymer Post Insulators in High Voltage Electrical Switches, *Journal of Performance of Constructed Facilities*, 30(5).

SAP2000 V19.2.1 Integrated Software for Structural Analysis and Design, Computers and Structures, Inc., USA.

Takhirov, S., Fenves, G., and Fujisaki, E. (2005), Seismic Qualification and Fragility Testing of Line Break 550 kV Disconnect Switches, *Pacific Earthquake Engineering Research Center University of California*, Berkeley, and PEER.

Takhirov, S. Blalock, F. and Stewart, J. (2017) Experimental Evaluation of System Level Properties of Porcelain Post Insulators Based on a Large Set of Full-Scale High-Voltage Insulators, *7th International Conference on Advances in Experimental Structural Engineering,* September 6-8, Pavia, Italy.

Tang, A. K. (2000), Izmit (Kocaeli), Turkey, Earthquake of August 17, 1999 Including Duzce Earthquake of November 12, 1999: Lifeline Performance, Technical Council of Lifeline Earthquake Engineering of ASCE, United States.